AIAA 79-1210R

Linear Analysis of Forced Longitudinal Waves in Rocket Motor Chambers

Michael M. Micci,* Leonard H. Caveny,† and William A. Sirignano‡
Princeton University, Princeton, N.J.

A methodology centered around the forced longitudinal wave (FLW) motor is being developed to investigate dynamic responses of rocket motors. The FLW motor establishes periodic longitudinal pressure and velocity oscillations in solid propellant rocket chambers. A linear analysis was developed to study propellant pressure- and velocity-coupled responses using dynamic pressure measurements at several locations in a motor. The analysis uses pressure amplitude and phase measurements. Variations in the propellant reponses are shown to produce measurable changes in the calculated oscillating pressures with velocity-coupled responses showing the greatest promise for determination from experimental data. Experimentally deduced velocity-coupled response functions are examined over a frequency range centered around the chamber fundamental mode for a range of interior flowfields and chamber pressures for 86%AP-14%HTPB propellants.

Nomenclature

a = speed of sound
A = chamber cross-sectional area
b = chamber burning perimeter
C_p = specific heat at constant pressure
C_v = specific heat at constant volume
e_0 = stagnation internal energy of combustion products
h_0 = stagnation enthalpy of combustion products
m_b = mass injection rate per area
p = pressure
R = universal gas constant
R_b = propellant response function
R_p = propellant pressure-coupled response function
R_v = propellant velocity-coupled response function
t = time
T = temperature
ΔT = nonisentropic flame temperature contribution
u = velocity
u_b = mass injection velocity
x = distance
α = growth constant
γ = ratio of specific heats
ρ = density
ϕ = phase angle

Superscripts

$( )'$ = fluctuating quantity
$\bar{( )}$ = mean quantity

Introduction

PRESENTLY, several organizations are working on devices for the experimental determination of pressure- and velocity-coupled response functions.[1] It was demonstrated that longitudinal pressure and velocity oscillations which are sinusoidal in time can be generated in a high loading density rocket motor[2] by modulating the outflow through a sonic nozzle (Fig. 1). In order to determine whether pressure measurements at several locations in the chamber can provide information about the dynamic response of the propellant to pressure and velocity oscillations, a linear analysis of the forced longitudinal wave (FLW) motor was developed. The development and initial application of the linear model is the subject of this paper.

Presented as Paper 79-1210 at AIAA/SAE/ASME 15th Joint Propulsion Conference, Las Vegas, Nev., June 18-20, 1979; submitted Aug. 23, 1979; revision received July 21, 1980.

*Ph.D. Candidate, Mechanical and Aerospace Engineering Dept. Student Member AIAA.

†Senior Professional Staff Member, Mechanical and Aerospace Engineering Dept.; presently with AFOSR/NA, Bolling AFB, Washington, D.C. Associate Fellow AIAA.

‡Professor, Mechanical and Aerospace Engineering Dept.; presently with Carnegie-Mellon University, Pittsburgh, Pa. Member AIAA.

Linear Analysis

A linearized analysis was developed to interpret measured dynamic pressures with forcing frequency, chamber geometry, mean flow chamber conditions, and propellant response functions. The model assumes one-dimensional flow in a constant area axisymmetric chamber with maximum Mach number sufficiently low (e.g., 0.1) such that terms of the order of M^2 or higher can be neglected. Flow turning losses are considered but gas phase and particulate damping are not incorporated into the model at this time. The flow properties are left in their dimensional form and any self-consistent set of units can be used. The conservation equations for mass, momentum, and energy are

$$\frac{\partial \rho}{\partial t} + \frac{\rho \partial u}{\partial x} + \frac{u \partial \rho}{\partial x} = \frac{b}{A} m_b(p,u) \tag{1}$$

$$\frac{\partial (\rho u)}{\partial t} + \frac{\partial (\rho u^2)}{\partial x} + \frac{\partial p}{\partial x} = 0 \tag{2}$$

$$\frac{\partial \rho e_0}{\partial t} + \frac{\partial \rho u e_0}{\partial x} + \frac{\partial p u}{\partial x} = h_0 m_b \frac{b}{A} \tag{3}$$

The perfect gas law is used

$$p = \rho R T \tag{4}$$

Subtracting u times continuity from the momentum equation (2) yields

$$\frac{\rho \partial u}{\partial t} + \frac{\rho u \partial u}{\partial x} + \frac{\partial p}{\partial x} + u(b/A) m_b(p,u) = 0 \tag{5}$$

Subtract u times momentum and $u^2/2$ times continuity from the energy equation (3) and separate e_0 into internal and

kinetic energy to obtain

$$c_v \frac{\partial \rho T}{\partial t} + c_v \frac{\partial \rho u T}{\partial x} + \frac{p \partial u}{\partial x} = (b/A) m_b [h_0 + u^2 - u^2/2] \quad (6)$$

Substitute the perfect gas law [Eq. (4)] and $h_0 = C_p (T + \Delta T) + u_b^2/2$ into the energy equation (6) to obtain

$$\frac{\partial p}{\partial t} + \frac{u \partial p}{\partial x} + \frac{\gamma p \partial u}{\partial x} = (b/A) m_b [a^2 + \gamma R \Delta T + (R/2c_v)(u_b^2 + u^2)] \quad (7)$$

The equations are now linearized by substituting $p = \bar{p} + p'$, $u = \bar{u} + u'$, etc. Terms of the order of $\bar{u}^2$ or higher are neglected. The momentum equation (5) becomes

$$\bar{\rho} \frac{\partial u'}{\partial t} + \bar{\rho} u' \frac{\partial \bar{u}}{\partial x} + \bar{\rho} \bar{u} \frac{\partial u'}{\partial x} + \frac{\partial p'}{\partial x} + u' \frac{b}{A} \bar{m}_b = 0 \quad (8)$$

The energy equation (7) becomes

$$\frac{\partial p'}{\partial t} + \bar{u} \frac{\partial p'}{\partial x} + u' \frac{\partial \bar{p}}{\partial x} + \gamma \bar{p} \frac{\partial u'}{\partial x} + p' \frac{\partial \bar{u}}{\partial x} = \bar{a}^2 \frac{b}{A} \bar{m}_b \sum_{p,v} \left[\frac{\bar{m}_b'}{\bar{m}_b} + \frac{\Delta T'}{\bar{T}} \right] \quad (9)$$

Defining the pressure-coupled and velocity-coupled response functions as

$$R_p = [m_b'/\bar{m}_b + \Delta T'/\bar{T}]/(p'/\bar{p}) \quad (10a)$$

$$R_v = [m_b'/\bar{m}_b + \Delta T'/\bar{T}]/(u'/\bar{a}) \quad (10b)$$

the energy equation (9) can now be written

$$\frac{\partial p'}{\partial t} + \bar{u} \frac{\partial p'}{\partial x} + u' \frac{\partial \bar{p}}{\partial x} + \gamma \bar{p} \frac{\partial u'}{\partial x} + p' \frac{\partial \bar{u}}{\partial x} = \bar{a}^2 \frac{b}{A} \bar{m}_b \left[R_p \frac{p'}{\bar{p}} + R_v \frac{u'}{\bar{a}} \right] \quad (11)$$

where the effects of pressure and velocity coupling are assumed to be additive.

Up to this point the analysis follows that of Culick.[3,4] Culick went on to solve the nonhomogeneous wave equation for the exponential growth or decay constant of a standing wave at the rocket chamber fundamental mode. The FLW motor imposes a nearly constant amplitude standing wave in the port of the rocket motor; pressure amplitude and phase measurements are made at three locations along the grain. The values of $p'/\bar{p}$ were typically in the range of 0.01-0.03. To take advantage of these measurements the first-order momentum and energy equations were integrated from the head of the motor where the initial conditions are known (p' is measured and u' is zero) down the port of the motor to any of the downstream pressure transducer locations. Measured chamber pressure oscillations are analyzed using a fast Fourier transform[5] to separate the amplitude and phase of the response to the forcing frequency from the higher harmonics and background noise. Using the linear analysis permits extraction of the response at the forcing frequency from the data and application to the model by the superposition principle. The oscillations extracted by the Fourier transform are sinusoidal in time and the two coupled first-order partial differential equations become ordinary differential equations. Kuentzmann at ONERA[6] has taken a similar approach to the solution of the linear equations but used the perturbed throat area as the downstream boundary condition. Because the FLW linear equations are integrated to a point upstream of the nozzle, no knowledge of the nozzle admittance is required. The FLW linear model is integrated numerically using a fourth-order Runge-Kutta scheme. The steady-state equations for mass, momentum, energy, and state were integrated by the same method. The response functions were assumed to have constant values throughout the chamber. As better methods of determining pressure- and velocity-coupled responses are developed, questions concerning the interdependency between pressure and velocity coupling can be addressed. However, currently in the analysis interactions between pressure and velocity coupling were not considered.

The flowfield dependency (and thus device dependency) of velocity coupling was recently emphasized by Price.[7] We concur with his statement of the complexities of the flowfield. The approach described in this paper is intended to produce data that are consistent with the state-of-the-art of the linear stability prediction program[8] which assumes that the values of the response functions are constant throughout the chamber. In carrying out this research we are providing data that will help to elucidate the mechanism of velocity coupling.

Parametric Study

Solutions calculated with the linear model for the case of no propellant dynamic response yielded standing waves similar to those in a closed-closed organ pipe except as modified by the mean flow. The real and imaginary parts of the pressure- and velocity-coupled response functions were then systematically varied to perform a parametric study. The purpose was to determine whether significant changes in a component of a response function produce measurable changes in the dynamic pressure at one or more of the transducer locations.

First, the pressure-coupled response was varied while the velocity-coupled response was held constant. The initial conditions, mean flowfield, and forcing frequency were identical for all the solutions. Since the analysis is linear, it is the ratio of amplitudes between two stations which is of interest. Changing the amplitude of the initial condition does not affect the ratio of amplitudes or the phase angle between any two stations. Thus the ratio of the amplitude of the oscillation at the location of interest to the amplitude of the oscillation at the head end of the motor is used in place of any absolute amplitude. It was found that relatively large variations in the pressure-coupled response were required to produce measurable changes in either the pressure amplitude or phase at either the midsection or nozzle transducer locations. It was also learned that for certain values of the imaginary part, changes in the real part had no effect on the dynamic pressure measured at the transducer locations. And the correspondence between a response function component and a pressure measurement in many cases was not unique. Similar behavior has been observed when the impedance tube is utilized for the measurement of a pressure-coupled response.[9] Thus it is believed that the FLW data interpreted by the linear analysis cannot be used to deduce accurately

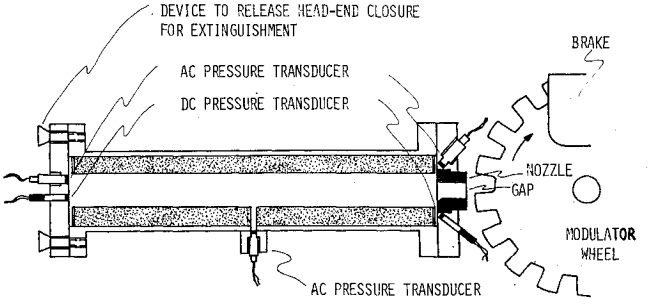

Fig. 1 Apparatus to excite longitudinal waves in rocket motor.

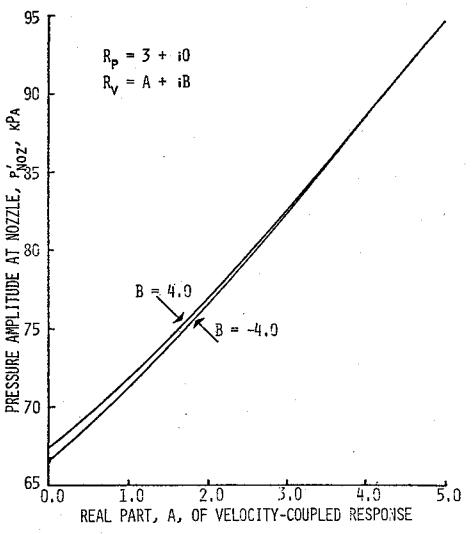

a) Changes in real part of velocity-coupled response produce measurable changes in pressure amplitude at nozzle for fixed head amplitude.

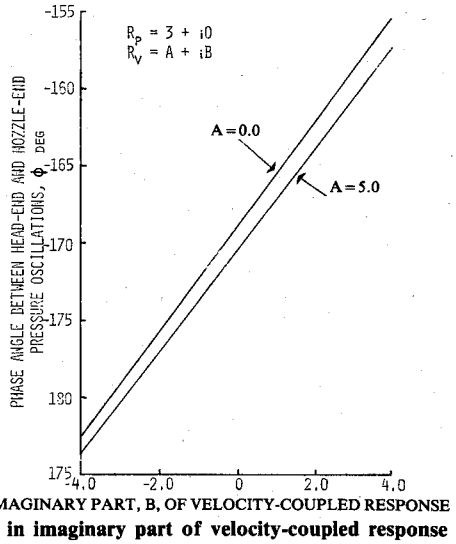

b) Changes in imaginary part of velocity-coupled response produce measurable changes in phase angle.

Fig. 2 Real and imaginary parts of velocity-coupled response affect calculated pressures at head and nozzle ends of rocket chamber.

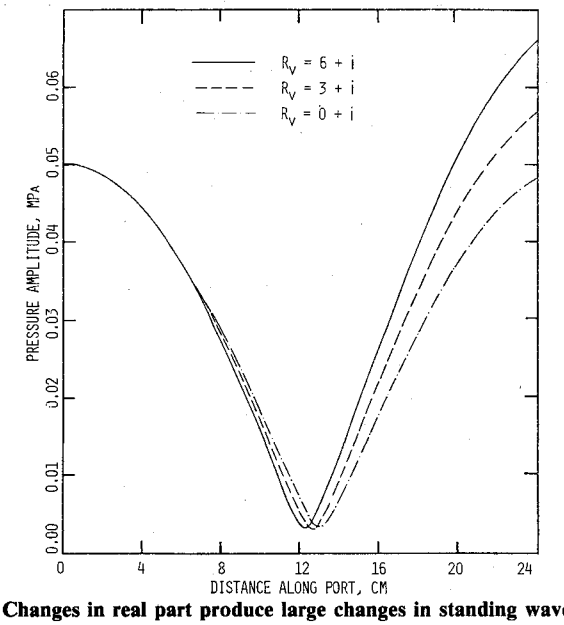

a) Changes in real part produce large changes in standing wave amplitude at nozzle end.

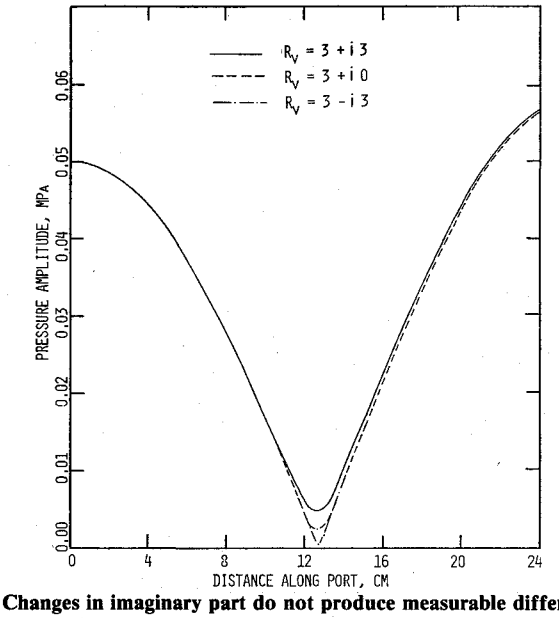

b) Changes in imaginary part do not produce measurable differences in standing wave amplitude.

Fig. 3 Effect of velocity-coupled response on pressure amplitude in rocket chamber.

pressure-coupled responses in experiments conducted with pressure measurements made at three locations along the grain.

Second, the velocity-coupled response was varied with the pressure-coupled response held constant. Figure 2a shows the effect of the real part of the velocity-coupled response on the pressure amplitude ratio from the head to the nozzle of the motor. It was found that changes in the real part produced changes in the amplitude ratio an order of magnitude greater than those produced by changes in the pressure-coupled response. The magnitude of this change is not affected by off-resonance operation. It can be seen from Fig. 2a that a variation in the imaginary part has a negligible effect on the amplitude ratio. The effect of a change in the real part on the amplitude of the standing pressure wave is shown in Fig. 3a. The full extent of the effect caused by the real part does not manifest itself until one approaches the pressure antinode at the nozzle end of the motor. Figure 3b shows that the imaginary part of the velocity-coupled response has no measurable effect on the amplitude of the standing wave except at the pressure node.

When the imaginary part of the velocity-coupled response was varied individually it was found that the phase angle between the pressure oscillations at the head and nozzle ends of the motor was affected linearly (Fig. 2b). As was the case for the real part, phase angle measurements currently obtainable (1 deg accuracy) would permit a measurement of the imaginary part of the velocity-coupled response. A change in the real part simply translates the line without affecting the slope. Figure 4a shows the effect of a change in the imaginary part on the phase angle of the standing wave pressure oscillations. The change in the phase angle becomes apparent only downstream of the pressure node. Figure 4b shows that variations in the real part of the velocity-coupled response have a very small effect on the pressure phase angle.

The physical cause of the insensitivity of the standing wave mode structure to the pressure-coupled response function is as follows. The linear model has shown that the standing wave mode structure is a very strong function of the velocity-coupled response but is a very weak function of the pressure-coupled response. This behavior does not change as one passes from 20% below the chamber resonant frequency to

20% above it. As shown by Culick[3] the growth or decay constant for acoustic waves α in a region from x_1 to x_2 is proportional to

$$\int_{x_1}^{x_2} |p'||R_b'|\cos\phi dx$$

where R_b' is the response of the propellant to pressure and/or velocity oscillations and ϕ is the phase angle between p' and R_b'. This is equivalent to integrating the dot product of the complex vectors p' and R_b'. Integrated down the entire chamber length, a positive integral simply means that the amplitude of the acoustic standing wave in the chamber will increase with time. The linear analysis has shown that in order to change the structure of the standing wave mode there must exist an asymmetry of the integrand on each side of the pressure node. By considering individually the pressure- and velocity-coupling portions of the integral, the contribution of each can be examined. The real part of the responses R_p and R_v is defined to be in phase with the perturbing force. For pressure coupling $R_b'=p'R_p$ and α for the entire motor is proportional to

$$\int_0^L |p'|^2 Re(R_p)dx$$

since the phase angle is zero. $|p'|^2$ is always positive and thus the pressure coupling contribution to the integral is either driving (i.e., positive) everywhere in the rocket motor chamber or damping everywhere. The integrand is symmetric with respect to the pressure node. For velocity coupling $R_b'=u'R_v$ and α for the entire motor is proportional to

$$\int_0^L |p'||u'R_v|\cos\phi dx$$

The contributions to the integrand due to the real and imaginary parts of R_v are now considered individually and $\tilde{\phi}$ is defined to be the phase angle between p' and u'. The integrand $|p'||u'|Re(R_v)\cos\tilde{\phi}$ is asymmetric (monotone increasing or decreasing) and the integrand $|p'||u'|\mathrm{Im}(R_v)\cos(\tilde{\phi}-\pi/2)$ is antisymmetric [approximated by $\sin(2\pi x/L)$]. $|p'||u'|\mathrm{Im}(R_v)\cos(\tilde{\phi}-\pi/2)$ integrated over the entire chamber length is close to zero because of equal positive and negative contributions to the integral. An asymmetric integrand produces a strong amplitude differential as shown in Fig. 3a and as antisymmetric integral produces a definite phase shift for the standing wave measured at the two pressure antinodes as shown in Fig. 4a.

Pressure coupling, whose contribution to the standing wave growth constant is either everywhere positive or everywhere negative, has little effect on the mode structure. Velocity coupling, whose contributions are either asymmetric or antisymmetric from one side of the pressure node to the other side, influences the mode structure to a much greater extent. Even at resonance, where the velocity coupling integral due to the imaginary part of the response function goes to zero because of equal positive and negative contributions, the antisymmetry still exists and the influence of velocity coupling on the mode structure remains strong. To prove that an asymmetric integrand produces a mode structure change, the sign of the pressure- and velocity-coupled response functions was intentionally switched on passing through the pressure node. This produced a symmetric velocity-coupling integrand and an asymmetric pressure-coupling integrand. In this instance the mode structure became a very strong function of the pressure-coupled response and a very weak function of the velocity-coupled response, thus demonstrating that it is the asymmetry of the integrand $p'R_b'$ and not its magnitude which determines the influence of the response functions on the acoustic standing wave mode structure.

Thus it was found that the pressure amplitude ratio from the head to the nozzle of the motor is almost solely a function

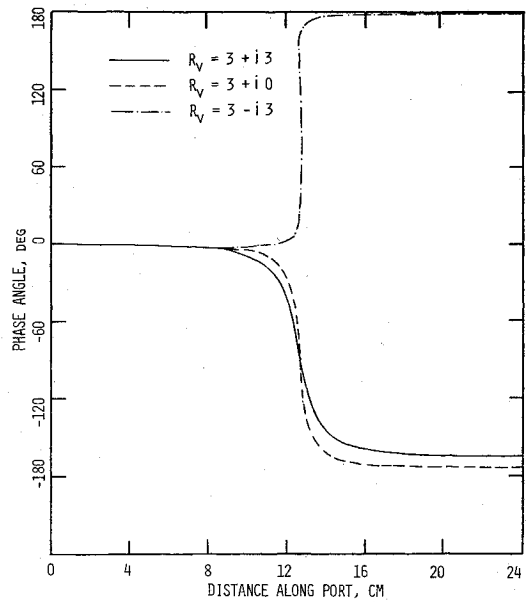

a) Changes in imaginary part produce measurable changes in phase angle past pressure node.

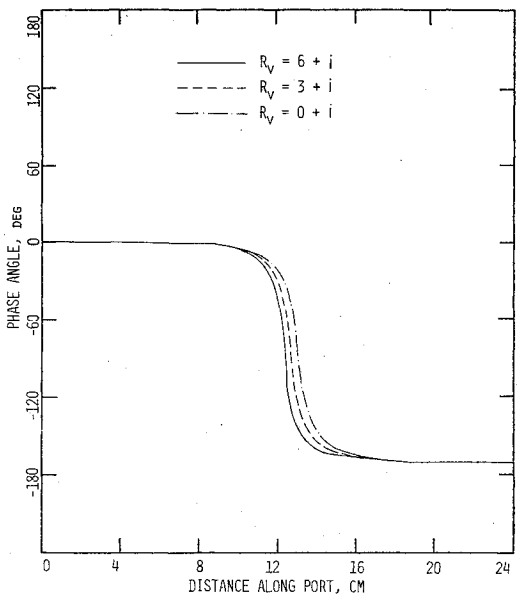

b) Changes in real part of velocity-coupled response do not produce measurable changes in standing wave phase angle.

Fig. 4 Effect of velocity-coupled response on phase angle between pressure oscillations in rocket chamber.

of the real part of the velocity-coupled response; the phase angle between head and nozzle pressure oscillations is almost solely a function of the imaginary part. This separation of interactions significantly simplifies the interpretation of the data. Portions of this parametric study were duplicated by Brown[10] using a similar linear model of the same order[11] and agreement between the two independent calculations was excellent. The possibility therefore exists for the deduction of a propellant velocity-coupled response function from dynamic pressure measurements made at only two locations in a rocket motor. The flow chart for accomplishing this is shown in Fig. 5. The pressure-coupled function would be assumed known. In practice, only an approximate value of the pressure-coupled response is needed due to the demonstrated insensitivity of the standing wave mode structure to pressure coupling. Real and imaginary parts of the velocity-coupled response which reproduce in the linear model the measured pressure amplitude ratio and phase angle can then be obtained.

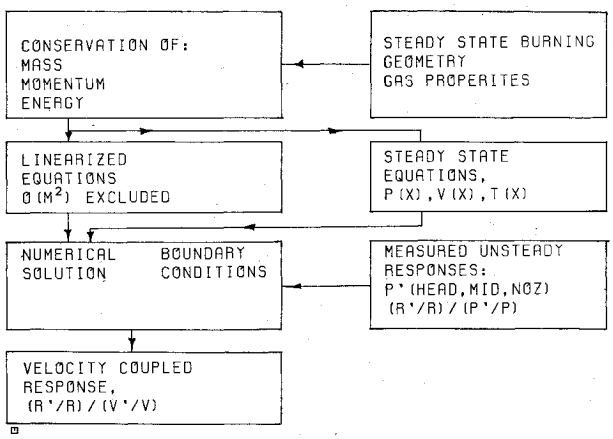

Fig. 5 Deduction of velocity-coupled responses from dynamic pressure measurements.

Table 1 Propellant formulation and properties

	Formulation a	Formulation b
Binder, HTPB, %	14.0	13.5
Ammonium perchlorate, %	86.0	86.5
15μm, %	20	—
45μm, %	40	20
180μm, %	40	20
400μm, %	—	60
Density, g/cm³	1.68	1.68
Strand burning rate at 6.9 MPa, cm/s	1.25	0.84
Exponent	0.43	0.60

Experimental Results

Several series of motor firings were conducted to determine whether the standing wave behavior predicted by the linear model agrees with the pressure measurements made in the motor and whether velocity-coupled response functions can be deduced from pressure measurements made at the head and nozzle ends of the motor. The propellant formulations tested are listed in Table 1. The FLW motor can accommodate a 25 cm grain with a fundamental frequency of approximately 2100 Hz or a 35 cm grain with a fundamental frequency of approximately 1500 Hz. Figure 6 shows pressure amplitude ratio and phase measurements made at the head, midsection, and nozzle end of a rocket motor for three identical 35 cm neutral burning star port grains cast from propellant formulation a. Figure 6a shows the pressure amplitude ratio of the nozzle to the head end of the motor. The decrease of the amplitude ratio as frequency decreases is a result of the pressure node moving past the nozzle end of the motor. Figure 6b, which plots the pressure amplitude ratio of the motor midsection to the head end as a function of frequency, shows the pressure node moving over the midsection transducer. The amplitude ratio reaches a minimum when the node is at the same location as the midsection transducer and gradually approaches one as the frequency approaches zero. Figure 6c reports the phase angle between the head and nozzle oscillations while Figure 6d shows the head-to-midsection phase angle. The head-to-nozzle phase angle remains in the vicinity of 180 deg, as expected for a standing wave. However, the head-to-midsection phase angle shifts from 180 to 0 deg as the pressure node moves past the midsection transducer. The behavior of the above four measurements as a function of frequency indicates that an acoustic standing wave is excited in the chamber port over the frequency range tested. This agrees with the linear model predictions over the same frequency range.

The FLW motor was then configured to obtain dynamic pressure data to be used in conjunction with the linear analysis to deduce the velocity-coupled response. The mid-

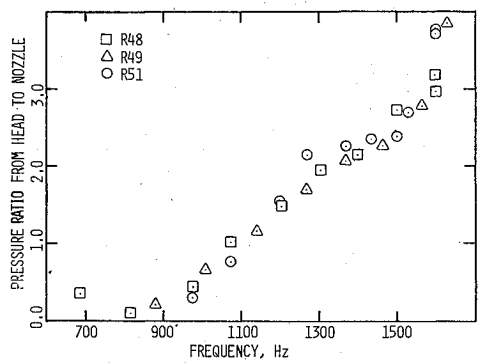

a) Pressure amplitude ratio from head to nozzle ends of motor.

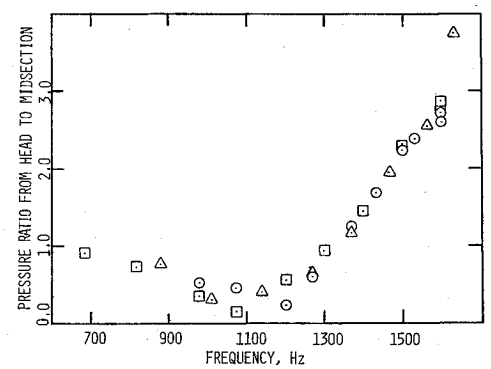

b) Pressure amplitude ratio from head to midsection of motor.

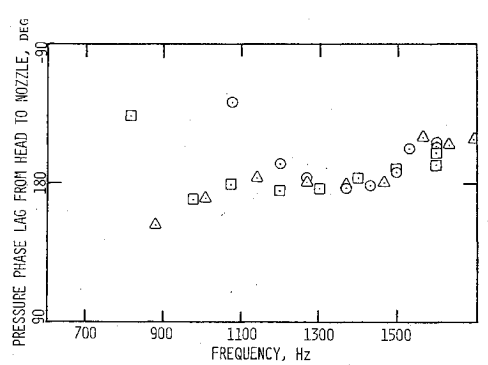

c) Phase angle between pressure oscillations at head and nozzle ends of motor.

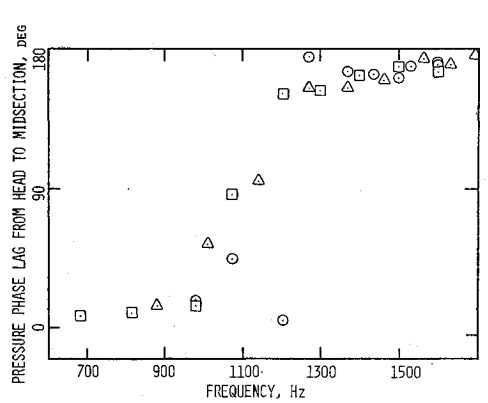

d) Phase angle between pressure oscillations at head and midsection of motor.

Fig. 6 Experimentally measured pressure gains and phases as function of frequency for three identical motor firings (R48, R49, and R51).

section pressure transducer was mounted at a location 2.5 cm upstream of the nozzle entrance where the nozzle pressure transducer is located. This permitted study of the effect of the flowfield on the velocity-coupled response. Real and imaginary parts of the velocity-coupled response would be

deduced assuming constant values of the response function using pressure measurements at the head and the location 2.5 cm upstream of the nozzle. An additional set of values for the response functions would be deduced using pressure measurements at the head and the nozzle entrance section. Any difference between the two sets of deduced response functions would indicate that the velocity-coupled response does vary with position down the port of the motor and therefore demonstrate a flowfield dependency. Since a measured pressure-coupled response was not available for the 86% solids AP-HTPB propellant, the pressure-coupled response function was calculated using the linearized Zeldovich method.[12] Figure 7 plots the calculated real and imaginary parts of the pressure-coupled response as a function of frequency at 5 MPa. Both the real and imaginary parts are required in the model.

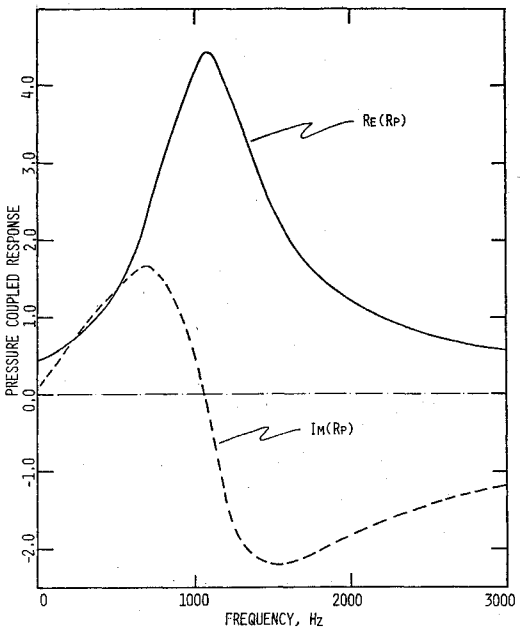

Fig. 7 Pressure-coupled response (real and imaginary parts) as calculated by linearized Zeldovich method.

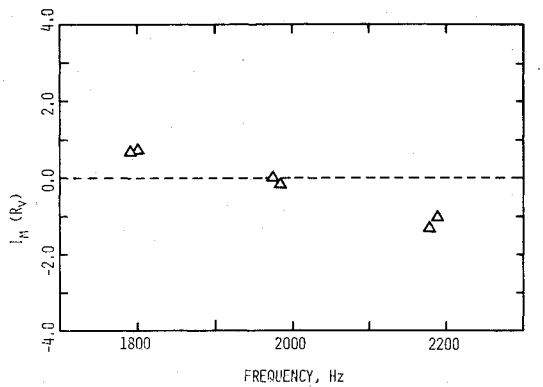

Fig. 8 Experimentally deduced imaginary part of velocity-coupled response as function of frequency for propellant formulation (a) showing run-to-run and batch-to-batch consistency.

Six motors 25 cm long with circular ports were fired with propellant formulation a and 21 motors with neutral burning star ports were fired with propellant formulation b, 12 in the 25 cm length and 9 in the 35 cm length. The chamber pressure for all the motor firings was near 5 MPa. Figure 8 plots the imaginary part of the velocity-coupled response vs frequency for propellant a. Figure 9 plots the imaginary part of the velocity-coupled response for propellant b. The four lowest frequency runs in Fig. 9 were obtained using the 35 cm long grain. The square symbols indicate values obtained by using pressure measurements taken at the head and 2.5 cm upstream of the nozzle. The triangular symbols mark values obtained by pressure measurements made at the head and nozzle entrance section. The Mach number at the nozzle entrance section is 15% higher than at the location 2.5 cm upstream. The data from each run were separated into up to 11 segments and analyzed individually with the linear model. Portions of any run where nonlinear oscillations or transients in the mean pressure became evident were eliminated and remaining segments were averaged and plotted on the figures. The size of the symbols indicates the accuracy with which the imaginary parts of the velocity-coupled response can be deduced from the pressure measurements for any individual data segment. A comparison of Figs. 8 and 9 indicates a differing trend with frequency for the two propellant formulations as would be suggested by the two AP oxidizer size distributions. Figures 8 and 9 show both run-to-run and batch-to-batch agreement. The close but nonsystematic relationship between the two values of the response function deduced at the differing Mach number locations indicates a random error and no discernable flowfield effect. The consistent results obtained for the imaginary part of the velocity-coupled response substantiate the ability of the FLW motor to provide data to allow the deduction of that component of the propellant response. Since a calculated pressure-coupled response function was utilized, a sensitivity study was conducted with the linear model. It was determined that an increase by a factor of two in the real part of the pressure-coupled response resulted in the real and imaginary parts of the velocity-coupled response increasing by no more than 25%. The insensitivity of the velocity-coupled response to large changes in the pressure-coupled response greatly simplifies interpretation of the data.

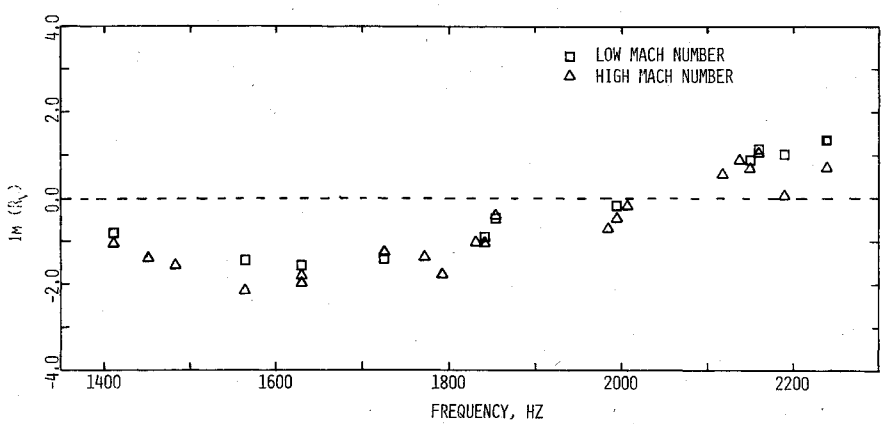

Fig. 9 Experimentally deduced imaginary part of velocity-coupled response as function of frequency for propellant formulation (b) showing agreement between response functions deduced from pressure measurements at two Mach numbers.

Conclusion

A linear analysis accurately interprets the behavior of the forced acoustic standing wave in the forced longitudinal wave (FLW) motor. A parametric study of the linear model has shown the possibility of deducing the real and imaginary parts of the velocity-coupled response from amplitude and phase measurements made at the head and nozzle ends of the rocket motor. It was determined from the linear model 1) that the pressure amplitude ratio from the head to the nozzle of the motor is almost solely a function of the real part of the velocity-coupled response, and 2) that the phase angle between head and nozzle oscillations is almost solely a function of the imaginary part. A sensitivity study demonstrated that a precise knowledge of the pressure-coupled response is not required for an accurate determination of the velocity-coupled response. Rocket motor experiments provided dynamic pressure amplitude ratio and phase data which were used to deduce consistent values of the imaginary part of the velocity-coupled response.

Acknowledgments

This research is being sponsored by the Air Force Office of Scientific Research. Major contributions to developing the digital data acquisition and FFT software were made by T. O. Williams and R. S Marlan. Fabrication of the test hardware, preparation of the propellants, and rocket motor testing were ably performed by C. R. Felsheim and S. O. Morris. The description of the analytical model benefited from discussions with R. S. Brown of Chemical Systems Division of United Technologies Corporation.

References

[1] Brown, R. S., Culick, F.E.C., and Zinn, B. T., "Experimental Methods for Combustion Admittance Measurements," *Experimental Diagnostics in Combustion of Solids*, Vol. 63, *Progress in Astronautics and Aeronautics*, AIAA, New York, 1978, pp. 191-220.

[2] Micci, M. M., Caveny, L. H., and Summerfield, M., "Solid Propellant Rocket Motor Responses Evaluated by Means of Forced Longitudinal Waves," AIAA Paper 77-974, July 1977.

[3] Culick, F.E.C., "The Stability of One-Dimensional Motions in a Rocket Motor," *Combustion Science and Technology*, Vol. 7, 1973, pp. 165-175.

[4] Culick, F.E.C., "Interactions Between the Flow Field, Combustion, and Wave Motions in Rocket Motors," NWC TP 5349, June 1972.

[5] Otnes, R. K. and Enochson, L., *Digital Time Series Analysis*, John Wiley & Sons, New York, 1972.

[6] Kuentzmann, P., "Recent ONERA Studies on Combustion Instabilities in Solid Propellant Rocket Motors," 53rd AGARD Symposium, April 1979.

[7] Price, E. W., "Velocity Coupling in Oscillatory Combustion of Solid Propellants," *AIAA Journal*, Vol. 17, July 1979, pp. 799-800.

[8] Lovine, R. L., "Standardized Stability Prediction Method for Solid Rocket Motors," AFRPL-TR-76-32, May 1976.

[9] Zinn, B. T., Salikuddin, M., Daniel, B. R., and Bell, W. A,, "Solid Propellant Admittance by the Driven Tube Method," AFOSR-TR-78-0548, Oct. 1977.

[10] Brown, R. S., personal communication, March 1979.

[11] Brown, R. S. and Waugh, R. C., "Pressure and Velocity Response Function Measurements by the Rotating Valve Method," 53rd AGARD Symposium, April 1979.

[12] Battista, R. A., Caveny, L. H., and Summerfield, M., "Non-Steady Combustion of Solid Propellants," Princeton Univ., Princeton, N.J., AMS Rept. 1049, Oct. 1972, p. 7-8.